NorthWest Research Associates, Inc.
P.O. Box 3027 • Bellevue, WA 98009-3027

NWRA-CR-92-R095 4 March 1993

LABORATORY STUDIES OF GRAVITY WAVE/ MEAN FLOW INTERACTIONS

ANNUAL REPORT FOR CONTRACT F49620-92-C-0005
FOR THE PERIOD 15 NOVEMBER 1991 TO 14 NOVEMBER 1992

Prepared by

Donald P. Delisi

Prepared for

Lt. Col. James G. Stobie
AFOSR/NL
Directorate of Life and Environmental Sciences
Building 410
Bolling AFB, DC 20332-6448

300-120th Ave. N.E. • Suite 220, Building 7 • Bellevue, WA 98005 • (206) 453-8141 • FAX (206) 646-9123

NWRA-CR-92-R095

4 March 1993

LABORATORY STUDIES OF GRAVITY WAVE/ MEAN FLOW INTERACTIONS

ANNUAL REPORT FOR CONTRACT F49620-92-C-0005
FOR THE PERIOD 15 NOVEMBER 1991 TO 14 NOVEMBER 1992

Prepared by

Donald P. Delisi

Prepared for

Lt. Col. James G. Stobie
AFOSR/NL
Directorate of Life and Environmental Sciences
Building 410
Bolling AFB, DC 20332-6448

REPORT DOCUMENTATION PAGE

Form Approved
OMB No 0704-0188

1. AGENCY USE ONLY (Leave blank)	2. REPORT DATE	3. REPORT TYPE AND DATES COVERED
	4 March 1993	15 Nov 91 to 14 Nov 92 / Annual

4. TITLE AND SUBTITLE

Laboratory Studies of Gravity Wave/Mean Flow Interactions

5. FUNDING NUMBERS

F49620-92-C-0005
UIC RF
3310
CS

6. AUTHOR(S)

Donald P. Delisi

7. PERFORMING ORGANIZATION NAME(S) AND ADDRESS(ES)

Northwest Research Associates, Inc.
PO Box 3027
Bellevue, WA. 98005

8. PERFORMING ORGANIZATION REPORT NUMBER

NWRA-CR-92-R095

9. SPONSORING/MONITORING AGENCY NAME(S) AND ADDRESS(ES)

AFOSR/NL
Directorate of Life and Environmental Sciences
Building 410
Bolling AFB, DC 20332-6448

10. SPONSORING/MONITORING AGENCY REPORT NUMBER

11. SUPPLEMENTARY NOTES

12a. DISTRIBUTION/AVAILABILITY STATEMENT

[illegible]

12b. DISTRIBUTION CODE

13. ABSTRACT *(Maximum 200 words)*

Progress is reported on laboratory measurements of gravity wave/critical layer interactions. Previous results have been reported for the interactions of single monochromatic waves propagating in a stratified fluid with a vertical velocity shear. The new results presented here are for two monochromatic forcing waves, each propagating with a different phase speed. Thus, the critical layer for each wave is distinct in the vertical.

The results for the two-wave case are compared to similar results for the one-wave case. In the one-wave case, only weak overturning appeared in the upper part of the tank for interaction times longer than about 13 minutes, and regular, periodic turbulence was observed in the lower part of the tank. In contrast, in the two-wave case, sustained overturning was observed in the upper part of the tank and packets of turbulence were seen in the lower part of the tank. Velocity profiles are currently being examined to attempt to understand these observed differences.

Other improvements in the hardware and software of the facility are also reported, and plans for the coming year are discussed.

14. SUBJECT TERMS	15. NUMBER OF PAGES
gravity wave, critical layer, internal wave, stratification, shear, turbulence	30
	16. PRICE CODE

17. SECURITY CLASSIFICATION OF REPORT	18. SECURITY CLASSIFICATION OF THIS PAGE	19. SECURITY CLASSIFICATION OF ABSTRACT	20. LIMITATION OF ABSTRACT
Unclassified	Unclassified	Unclassified	Unclassified

TABLE OF CONTENTS

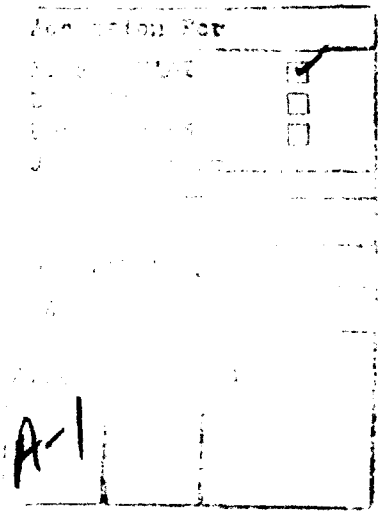

LIST OF FIGURES AND TABLES

1. Introduction

This report is the first annual report for contract number F49620-92-C-0005 from the Air Force Office of Scientific Research to Northwest Research Associates, Inc. The research area is laboratory studies of gravity wave/mean flow interactions. The period of performance covered by this report is 15 November 1991 to 14 November 1992.

The next section, Section 2, contains a review of gravity wave/mean flow interactions, with an emphasis on previous laboratory experiments. In Section 3, we discuss our experimental facility; in Section 4 we discuss our recent work and results over the past year. Section 5 contains our plans for the following year.

2. Background

Atmospheric gravity waves have a large range of length and time scales. They are important in atmospheric circulation for transporting momentum and for generating turbulence, thereby producing mixing. One mechanism for the breakdown of gravity waves into turbulence and mixing occurs as a wave approaches its critical level, where the mean flow equals the horizontal phase speed of the wave (Booker and Bretherton, 1967).

It is important to understand how gravity waves propagate and dissipate in the atmosphere to be able to predict atmospheric circulation. The interactions and couplings between large-scale and small-scale atmospheric phenomena are not well understood, and this lack of understanding explains, in part, our inability to predict atmospheric conditions globally or locally very far in advance. For example, studies have shown that terrain has a significant effect on the variance in the troposphere and the stratosphere (Nastrom et al, 1987) and that breaking gravity waves (such as might occur in gravity wave/critical layer interactions) are important in the large-scale flow in the troposphere and lower stratosphere. Hence, local topography generates mesoscale gravity waves, and these waves are important globally as well as locally.

Linear theory for the interaction of a gravity wave with a critical layer was first developed by Bretherton (1966) and Booker and Bretherton (1967). Subsequent theoretical and numerical research has been performed by Benney and Bergeron (1969), Maslowe (1973, 1977), Grimshaw (1975), Fritts (1978, 1979, 1982), Brown and Stewartson (1980), Dunkerton (1980, 1981, 1982), Lindzen (1981), Dunkerton and Fritts (1984), and many others. For reviews, see Fritts (1984), Maslowe (1986), and Andrews et al (1987).

Observationally, it has been difficult to locate and observe gravity wave/critical layer interactions in the atmosphere. To help understand this phenomenon, several gravity wave/critical layer experiments have been performed under controlled, laboratory conditions. Using monochromatic waves, laboratory experiments have been reported by Thorpe (1973, 1981), Koop (1981), and Koop and McGee (1986). In these experiments, the gravity waves were generated by a corrugated bottom floor. The interaction of a broadband gravity wave source with shear was also reported in Bretherton et al (1967) and, cited above, Koop (1981) and Koop

and McGee (1986). In these experiments, a triangular-shaped obstacle or a cylinder generated the broadband wave signal. In all these laboratory experiments:

(a) the results were primarily qualitative and were presented as flow visualization results or as point sensor temporal plots,

(b) due to limitations of the experimental facilities, only short-time (several minutes or less) gravity wave/critical layer interactions could be studied, and

(c) the horizontal wavelengths of the forced gravity waves were small, generally less than 15-25 cm, and, hence, viscosity may have been important in the overturning regions, where typical length scales are a fraction of the horizontal wavelength of the incoming wave.

Our own previously-reported laboratory study of gravity wave/critical layer interactions with monochromatic waves (Delisi and Dunkerton, 1989) differed from the above studies in three ways:

(a) we were the first to report quantitative measurements of the mean flow modifications due to the interactions,

(b) long-time interactions were reported, with observed interaction times of over an hour, and

(c) the forced gravity waves had a horizontal wavelength of 240 cm, an order of magnitude larger than previous studies.

In this study, we will expand on the results reported in Delisi and Dunkerton (1989) first by examining two monochromatic waves, each with its separate critical level, and, later, by investigating a compact, broadband wave source. Our first results with two monochromatic gravity waves are discussed in this report.

3. Review of the Experimental Facility

The experimental facility consists of an annular wave tank, computers to run the experiment and to acquire the probe measurements, power supplies and motor drivers to drive the forcing wave, and flow measurement and visualization equipment. To perform an experiment, the tank is filled with salt-stratified water, a lid is rotated on the water surface to generate a shear, and gravity waves are generated on the bottom floor of the tank by moving the floor vertically up and down. The gravity waves generated at the floor propagate up into the tank, reach a critical level where the current speed equals the phase speed of the wave, and interact with the mean flow. The interaction is measured with probes and observed with flow visualization.

The tank consists of two concentric acrylic walls, 1.8 and 1.2 m in diameter, and 40 cm high (Figure 1). The acrylic is attached to, and supported by, circular aluminum frames. The frames extend below the acrylic walls to support the floor actuation equipment. The floor membrane is made out of resilient, rubberized material used in scuba diving wetsuits.

Under the membrane are 32 pie-shaped pieces of acrylic, joined end to end to form a continuous ring. At the junction between each floor piece is a tee-shaped aluminum piston. The top of the tee runs along and supports the junction between adjacent pie-pieces, and the vertical portion extends downward. At the bottom of the tee is a ballnut. A ballshaft threads into the ballnut, and extends down to and through a flange bearing. By turning the ballshaft, the ballnut, the tee, and the associated section of the floor move up and down.

The ballshaft is coupled to a stepper motor via a drive belt. Each stepper motor has a stepper motor driver that receives its signals from a computer. The motors are powered by two 3-phase, 3000-watt DC power supplies. For fast response, the motors are driven through resistors that are 10 times the internal resistance of the motors.

The tank has a "lid" that is an acrylic ring of the same nominal dimension as the floor of the tank. The lid is used to generate the shear flow. It is trimmed for a loose fit into the tank. In shape it is flat like a large "O." The inner and outer perimeters have 5 cm high walls, so the lid can float on the water in the tank. The outer wall has a groove for a long rubber drive cord. Four brass spindles are located around the perimeter of the main tank, one being powered. The drive cord is passed around the lid, and pulled away from the lid to go outside the spindles. This centers the lid in the tank. The powered spindle makes the lid rotate.

In order to observe the interactions from a frame of reference moving with the waves, the tank has a rotating boom. The boom is driven by a variable-speed DC motor. The motor is capable of rotating the boom at speeds up to and greater than the speed of the fastest bottom wave. A platform attached to the boom contains a video camera, a 35-mm camera, and a shadowgraph light source.

Neutrally buoyant particles are placed in the flow prior to the tank being filled. The particles are illuminated in a thin, vertical sheet near the tank center line during an experiment. Time exposures of the particles by a 35-mm camera on the side of the tank yield streak photographs of the particle motions. These steak photographs yield vertical profiles of instantaneous particle velocity. The average of these vertical profiles over one wave period yields the mean velocity (Delisi and Dunkerton, 1989).

A Seabird Electronics Model SBE-7 microstructure conductivity probe extends into the tank from the side, making a right angle near the tank center line. The probe shaft on the outside of the tank is fastened to an arm. Moving the arm causes the probe shaft to rotate, moving the probe tip up and down in the tank. The arm is driven by a crank and pushrod connected to a variable speed gearmotor. The gearmotor also drives a position encoder that generates 512 square waves and one index pulse for each revolution of the encoder and, hence, for each cycle of the conductivity probe. These square waves and index pulses are stored by the data acquisition computer and are used in later analysis to determine density vs. probe depth.

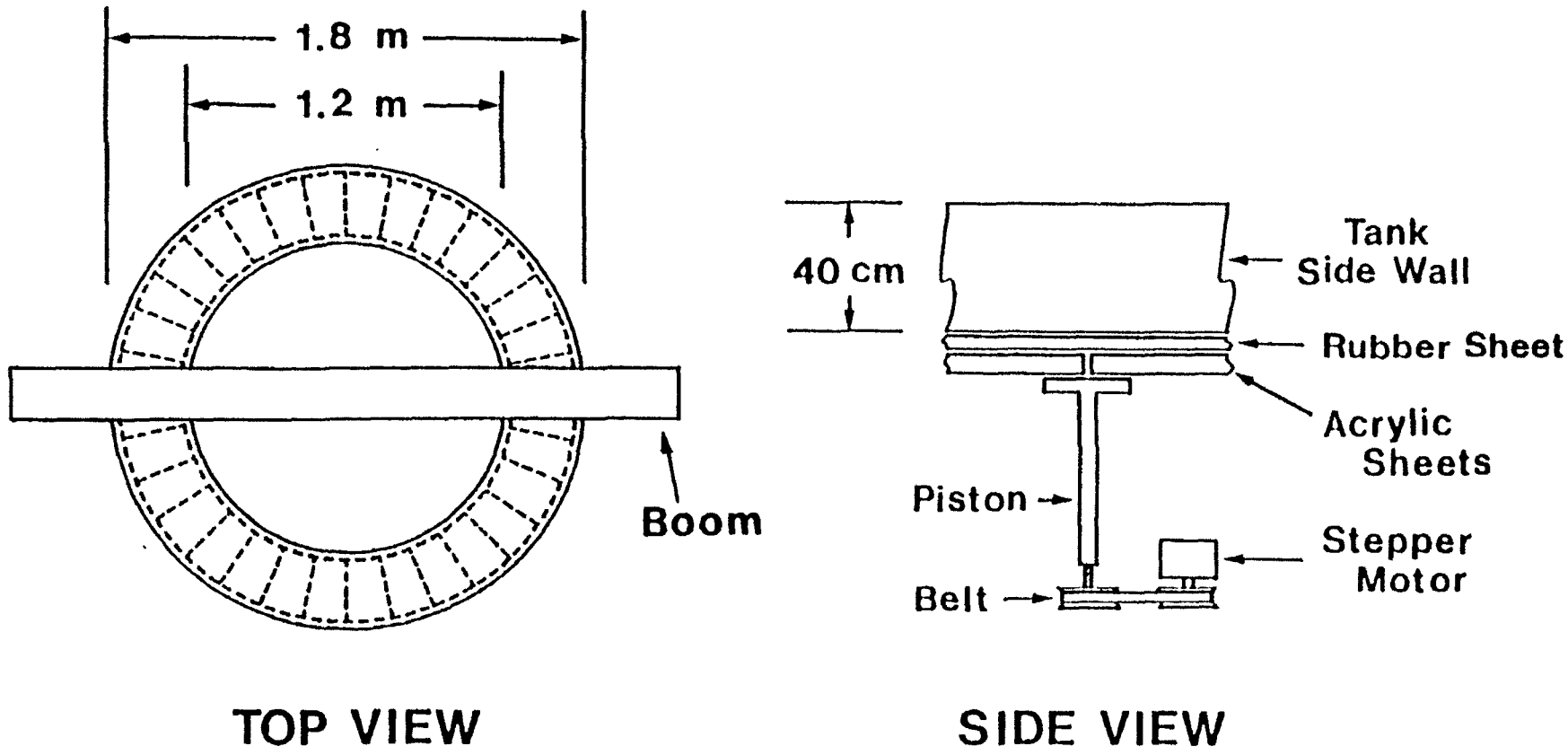

Figure 1. Top and side views of the experimental facility.

4. Work Performed in the Past Year

During the past year, work was performed in three areas: designing, building, and incorporating new hardware into the experimental facility; modifying the software which is used to control the experiments and to acquire the data; and performing gravity wave/critical layer experiments. Each of these areas is discussed below.

4.1 Hardware

Several new hardware features were added to the experimental facility this year. These features include new power supplies to drive the stepper motors and a new sensor to measure the vertical position of the bottom floor.

New power supplies were incorporated because the previous power supplies were running at their full capacity, and we were experiencing intermittent dropouts and motor failures. It was, therefore, determined that those power supplies would be incapable of consistent operation in the two-wave problem. Thus, new power supplies were deemed a requirement for successful completion of the two-wave study.

To understand the new power supplies, we will first describe how stepper motors work. Stepper motors, like any motors, require a certain current to exist in the windings to generate torque. Unlike ordinary motors, however, they operate over a wide speed range. When the motor is energized and motionless (an unusual condition for a motor), a certain voltage is needed to drive the required current. As the motor begins to rotate, a "back EMF" is generated proportional to motor speed. This "back" voltage opposes the applied voltage, effectively reducing it. This reduced net voltage drives only a reduced current through the motor. The reduced current yields reduced torque. The net effect is that available motor torque falls off rapidly with increasing motor speed.

The least expensive means of improving the speed-torque characteristics of a stepper motor is to place a resistor in series with the motor winding. Treating the motor winding/resistor combination as a unit, we see that a larger applied voltage is needed to drive the required motor current. Since the back voltage is still proportional only to speed, a much higher speed is required to effectively oppose the higher applied voltage.

In our application, the resistors were chosen to be about 10 times the internal resistance of the motors, and the applied voltage was chosen to drive the motors at 65 - 70% of rated current. This equals 10 ohms and 27 volts for one set of 22 motors, and 5 ohms and 20 volts for the other set of 10 motors. In this configuration, the resistors burn up about 50 watts apiece.

To supply this voltage, two power supplies were built, one for each set of motors. Each supply runs on 480 volt, 3-phase commercial power. Each supply consists of three 1000 va transformers wired to a full-wave 3-phase bridge rectifier. No filter capacitors are used. The hardware portion of each supply is identical. The different voltage outputs are achieved by different wiring schemes at the primaries and secondaries of the transformers. At present, the 27-volt supply is operating at 89% capacity, and the 20-volt supply at 47% capacity.

These new power supplies have been installed in the experimental facility and have been used in the experiments. To date, there have been no stepper motor dropouts or failures associated with these new power supplies.

In addition to the power supplies, one new sensor to measure floor position as a function of time was incorporated into the facility. This sensor was necessary due to the nature of the two-wave problem.

In the one-wave gravity wave/critical layer problem, we use only a single monochromatic wave as the forcing wave. Thus, each wave cycle looks like every other wave cycle. For wave number 2 and a phase speed of 4.5 cm/sec, the period of the bottom floor is 53.33 sec.

In the two-wave problem, we use two monochromatic waves as the forcing function. For wave number 2 and phase speeds of 4.5 and 3.5 cm/sec, the periods of the waves are 53.33 sec and 68.57 sec, respectively. Because these two waves beat together, the bottom floor repeats itself (at a fixed location) after eight minutes. To relate the conductivity and shadowgraph measurements to the position of the bottom floor in the wave cycle, we installed a position sensor on the bottom of the tank. This position sensor is a 10-turn potentiometer that is connected to the stepper motor/floor activator directly beneath the tip of the conductivity probe. The rotary motion that drives the floor up and down also turns the potentiometer by means of a friction wheel. The potentiometer is wired as a voltage divider to a regulated power supply, and the output from the potentiometer is proportional to the tank bottom position at that point. The output from the potentiometer is stored on the data acquisition computer simultaneously with the measurements from the conductivity probe.

4.2 Software

Software was developed and/or modified for two important purposes:

1) To control the stepper motors which move the bottom floor and simulate the propagation of one or two waves and

2) To collect data real-time on a personal computer (PC).

Each of these software programs will be briefly described.

In our earlier work, we developed the software to control the bottom floor stepper motors to simulate the propagation of a single wave. To perform two-wave experiments, we had to rewrite our software.

The new computer program to drive the bottom floor uses seven input parameters including wave direction, wavenumber, wave speed and wave height. The program can drive the stepper motors to propagate either one or two waves.

The program builds an array for each wave, the values of the array being the wave height (in centimeters, positive and negative). The computer moves a set of 32 equally-spaced pointers, one for each motor, through each array at a fixed rate. Thus, the size of the array determines the wave speed. If the two arrays are different sizes, the two waves will move at different speeds.

Three additional 32-value arrays are used in the program: one storing actual motor position, one storing the desired motor position, and one storing the difference. The desired motor position for a given motor is determined by adding the wave height from the first wave's array to the wave height from the second wave's array, using the two pointers associated with each motor.

The difference array (which is the distance each motor needs to move) is calculated by comparing actual position to desired position for each motor. For any motor, if the difference array value is zero, no motor steps are taken. If the array value is non-zero, a single step command (plus or minus) is issued to that motor, and the array value is decremented or incremented by one. The difference array is gone through repeatedly until, eventually, all 32 values in the array go to zero.

The speed at which the pointers move through the wave height arrays, and the speed at which the motors take steps, are determined by a delay loop in each operation. The values of the delay loops are computed by a procedure invoked at startup, using the computer's real-time clock.

The program can either start the waves running at full wave height or can perform a gradual start where the waveheights start at zero and ramp up to the maximum value after 4 revolutions around the tank.

The second real-time computer software program used in these experiments is a data collection program that runs on a separate computer from the one controlling the tank bottom. This program is a modification of software originally developed for use in another project. The software operates a DAS-8 Analog to Digital card (Metrabyte Instruments, Inc.), and collects and stores data associated with an experiment. The data collected and written are time (hour, minute, second, and centisecond), conductivity, tank bottom position at the location under the conductivity probe, probe encoder count (0 to 511), and probe index count (number of probe up-down cycles, incremented by the encoder index pulse).

4.3 Gravity Wave/Critical Layer Experiments

To perform an experiment, we fill the tank with a stratified salt water solution, rotate the lid at the water surface to create a shear profile, then propagate one or two waves on the bottom floor by moving the floor vertically with the stepper motors. Measurements consist of instantaneous density data from the oscillating conductivity probe, bottom floor position data, mean and instantaneous velocity profiles from the particle streak photographs, and 35-mm and video pictures of shadowgraph flow visualization which shows turbulent regions.

The velocity profile is nominally identical from run to run and is shown in Figure 2. The profile shows a nearly constant velocity in the upper layer, where the lid has mixed the fluid, followed by a nearly exponential velocity profile beneath the mixed region.

We used two, linearly stratified density layers in these experiments. The uppermost layer is a highly stratified region whose purpose is to minimize the depth of the mixed layer generated by

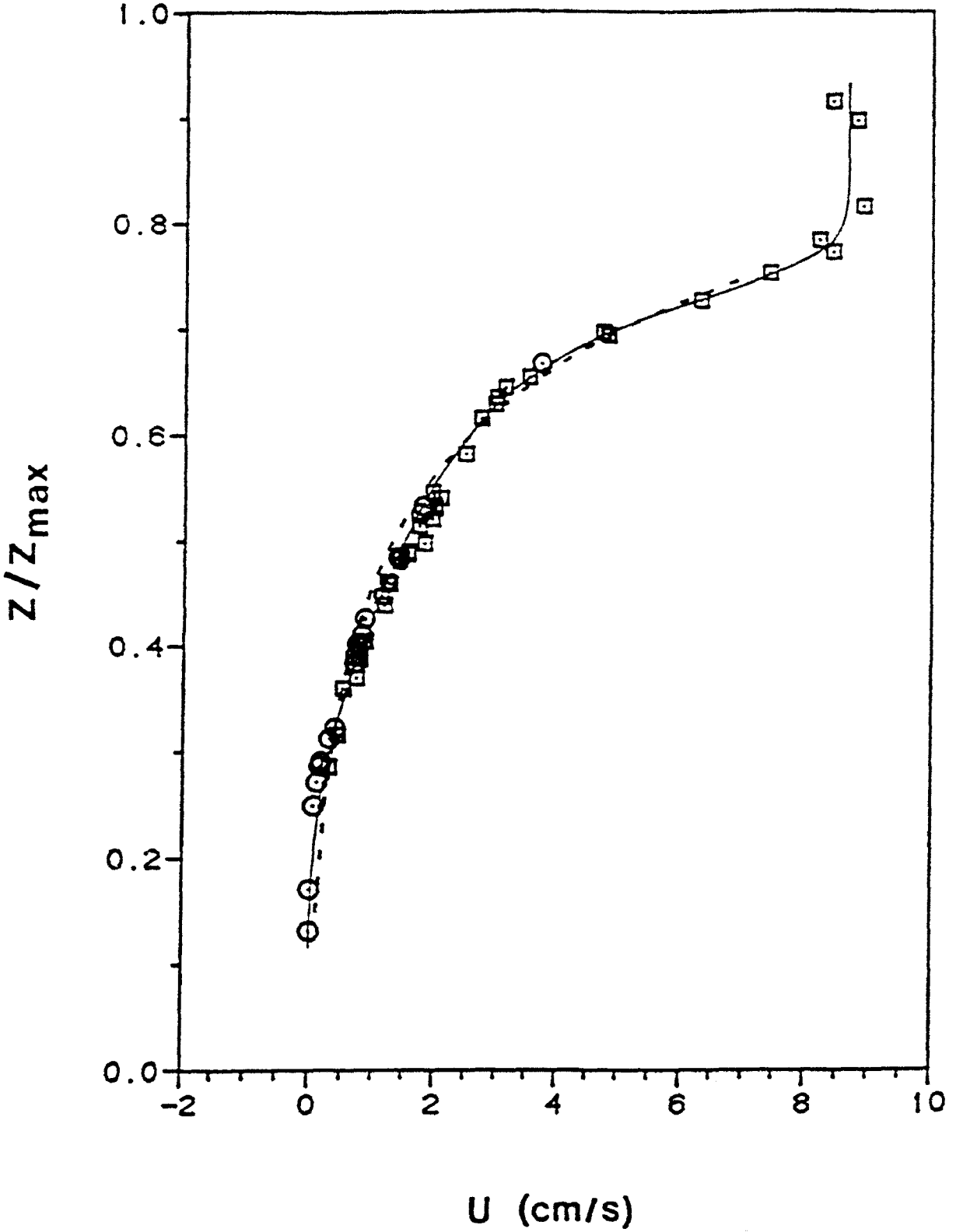

Figure 2. The velocity profile at the start of an experiment. The solid line is a subjective fit through the data. The dashed line is an exponential fit. Z is the height above the bottom floor; Z_{max} is the total water depth of 38.7 cm. (From Delisi and Dunkerton, 1989)

the rotating lid. The initial density profile for the two-wave experiment discussed below is shown in Figure 3. The Brunt-Vaisala frequency, N, for the top layer is 1.59 sec^{-1} where

$$N = - \left(\frac{g}{\bar{\rho}} \frac{\partial \rho}{\partial z} \right)^{1/2} \tag{1}$$

where g is the acceleration due to gravity, ρ is density, $\bar{\rho}$ is average density, and z is the vertical coordinate. The value of N in the lower layer is chosen from considerations of the dissipation scale height, d, given by

$$d - \frac{k \hat{c}^4}{\nu N^3} \tag{2}$$

where k is the zonal wave number, $\hat{c} = c - \bar{U}$, c is the phase speed of the forced wave at the bottom floor, $\bar{U}$ is the mean flow speed, and ν is the kinematic viscosity (Plumb and McEwan, 1978). To minimize gravity wave dissipation and to maximize the wave energy reaching a given vertical level, we want d to be as large as possible. For a given zonal wavenumber and phase speed, from eqn. (2), we want N to be as low as possible in the tank. For this reason, we have a weaker stratification and, hence, a lower value of N, at the bottom of the tank than at the top of the tank (Figure 3). In Figure 3, the value of N in the bottom layer is 0.82 sec^{-1}.

4.3.1 One Wave Results

Several one-wave, gravity wave/critical layer experiments were performed during the past year to check our new software and hardware, to check our experimental technique, and to act as repeatability checks on our previous results. The experiments we repeated were Case B in Delisi (1988), which is also similar to the results in Delisi and Dunkerton (1989).

The forcing wave we used on the bottom floor was a wavenumber two wave with an amplitude of 4.0 cm peak-to-peak and a phase speed of 4.5 cm/sec. The wave was not sinusoidal, but was asymmetric to match the propagating wavefronts in a nonsheared, linearly stratified fluid. Figure 4 shows the measured height of the bottom floor (at one motor location) over one cycle (solid line), the desired input wave function (dotted line), and a sine wave of the same amplitude (dashed line). There is good agreement between desired and measured waveheight. The asymmetry in the actual, measured wave increases as N in the bottom layer increases. This asymmetry in the forcing function is intended to mimic the generated gravity wave and to, therefore, reduce the higher harmonics that would be generated by using a sinusoidal wave on the bottom floor.

Figure 5 shows the measured height of the bottom floor at one location for an entire one-wave run. Note that the height of the bottom floor is periodic and repeats itself with a period of about 53.3 sec, which is the period of the forcing wave.

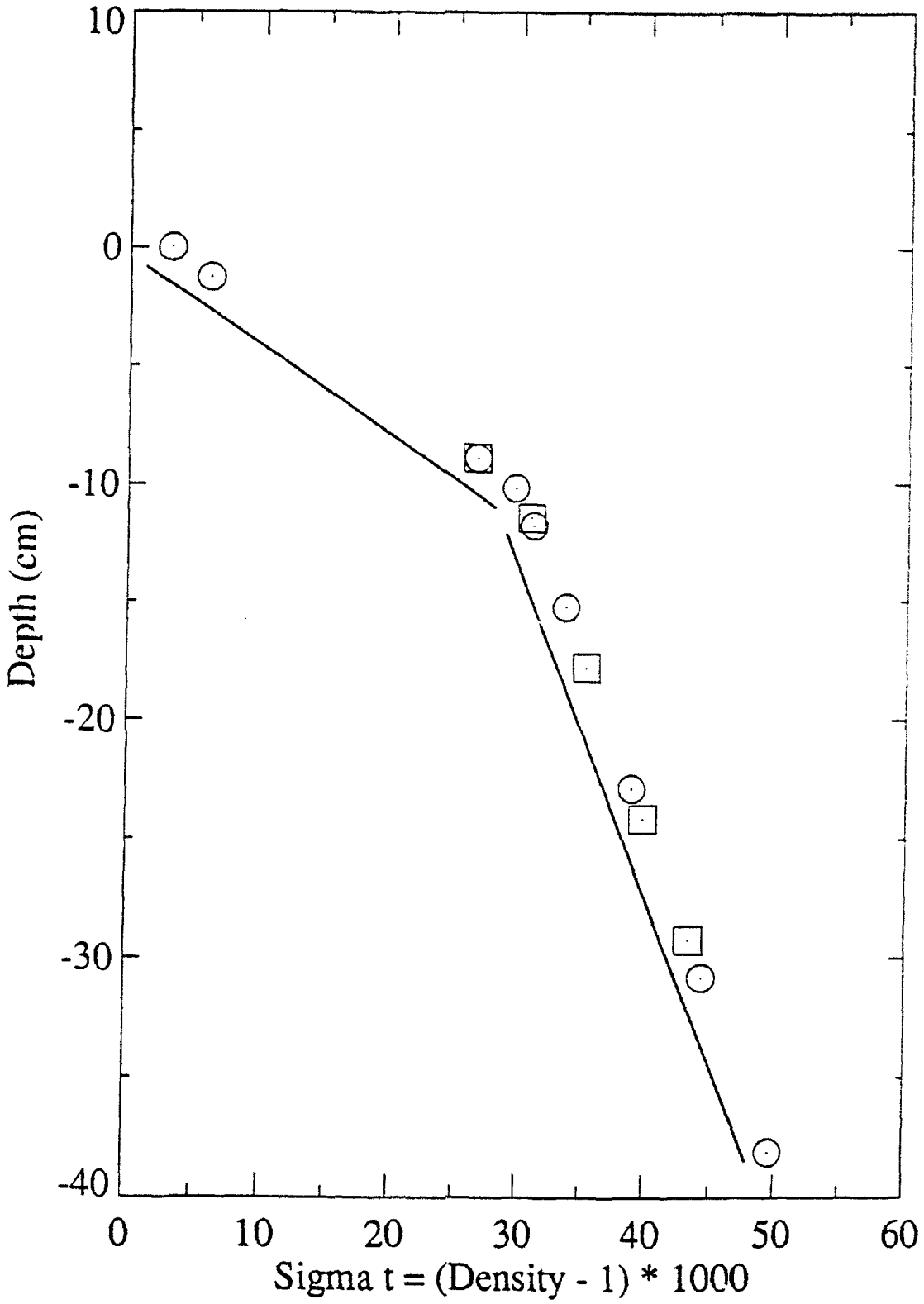

Figure 3. The measured initial density profile. Circles are values taken during the filling of the tank; squares are probe samples taken after filling the tank. Straight lines are drawn for comparison to linearity.

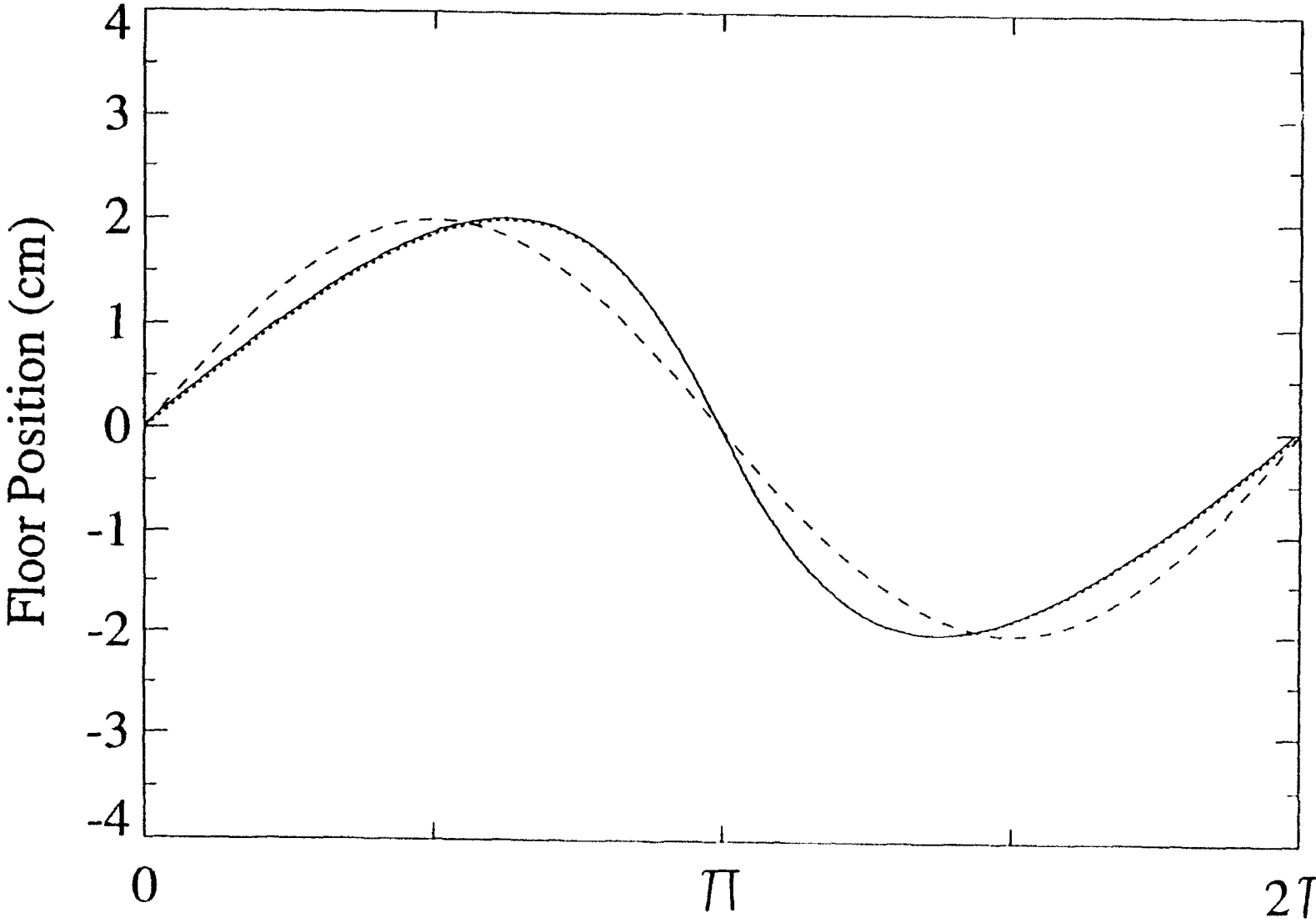

Figure 4. The asymmetric bottom floor wave. The dotted line is the desired wave, the solid line is the measured wave, and the dashed line is a sine wave.

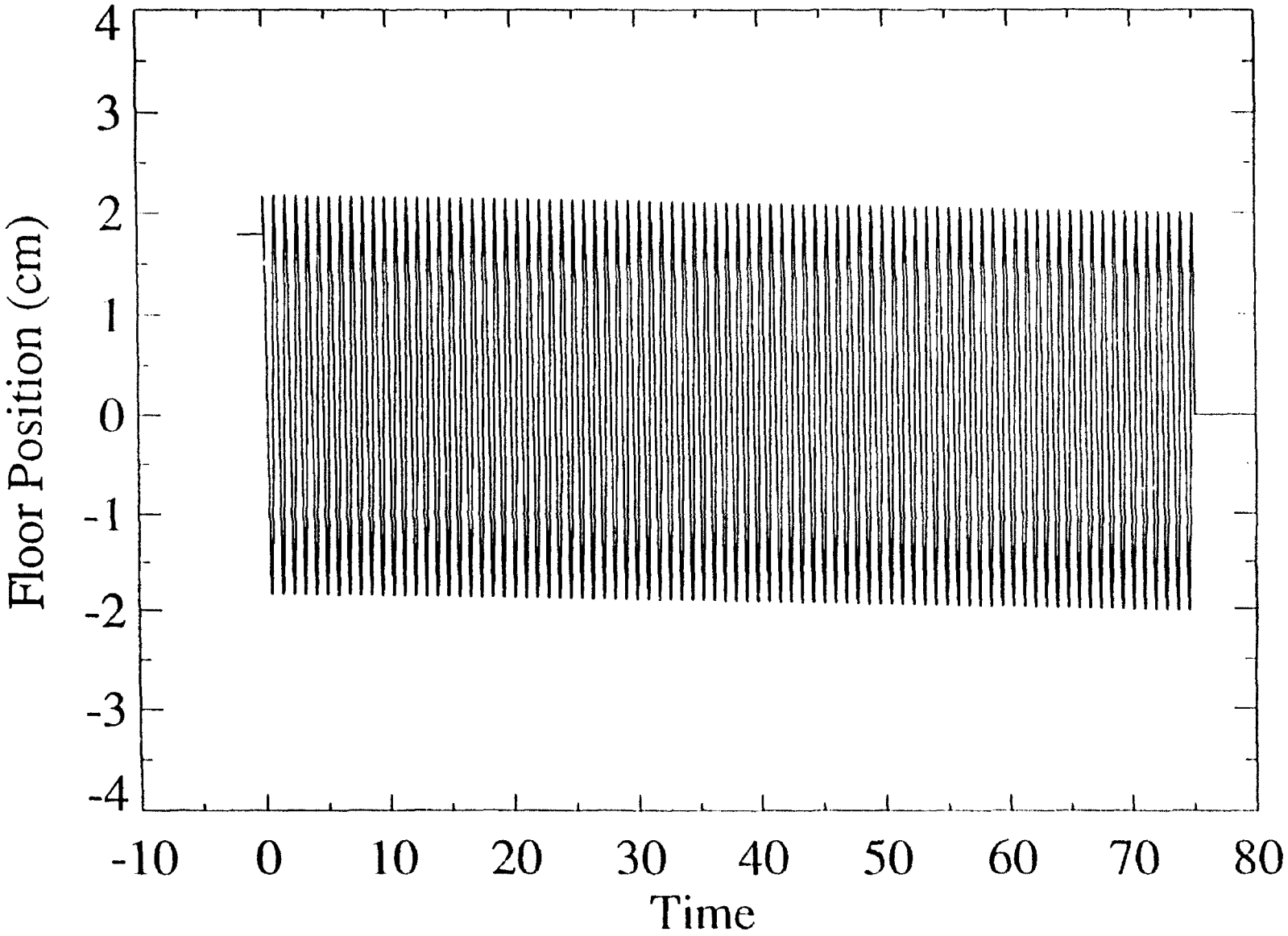

Figure 5. Measured floor position (cm) vs. time (sec) at one location for a one-wave run.

The shadowgraph is the primary flow visualization technique we use to visualize the breaking wave, turbulent regions (Delisi and Dunkerton, 1989). For the results presented here, the shadowgraph was fixed at one location and did not rotate around the tank. For the first 10-12 wave cycles, the breaking is Kelvin-Helmholtz (K-H) in nature, with overturning billows. The overturning first appears just below the critical level, and progresses downwards towards the floor. For each succeeding wave cycle in the first 10-12 wave cycles, the overturning region typically first appears closer to the floor than in the last cycle and the overturning region ends closer to the floor than in the preceding cycles. After the first 10-12 cycles, the character of the breaking changes from overturning K-H billows to the "wedge" discussed in Delisi and Dunkerton (1989).

Videotapes of these shadowgraph visualizations clearly show the regions of overturning and turbulence as a function of time. We have analyzed these videotapes to determine the vertical extent of the breaking regions as a function of time. The result for a one-wave experiment is shown in Figure 6. Here, we show depth in the tank vs. the time after the start of the experiment, where the dark, solid lines indicate the observed, turbulent regions. For example, at t = 4 min 50 sec, turbulence was observed between 12.7 and 15.5 cm depth. At t = 5 min, the turbulent region was observed lower in the tank, at depths between 15.2 and 17.8 cm. Note in Figure 6 that the overturning first appears near the top of the tank and progresses downwards, towards the bottom floor, from t = 0 to t ~ 13 min. This overturning is K-H in nature. For $t \gtrsim 13$ min, the observed turbulence occurs in "wedges," and is primarily in the bottom half of the tank, with only sporadic, patchy turbulence being observed in the top half of the tank.

We have analyzed the frequency of the observed turbulence in Figure 6 in two ways. First, we measured the observed time of the initial turbulence for each patch in Figure 6, using only the initial times of the wedges for t > 13 min. Defining the time between successive patches as Δt, we estimate the phase speed of the wave as $240/\Delta t$, where 240 cm is the wavelength of the wavenumber two waves used here (at the center of the annulus with a radius of 1.5 m). The results are shown in Figure 7. In this figure, we see that the average of the phase speed estimates is around 4.5 cm/sec, the input phase speed, except for t > 50 min, where we do not observe a turbulent region during each wave cycle. Looking at the videotapes and timing the wave crests and troughs, we estimate the observed wavespeed in the tank as 4.48 cm/sec, which is very close to the input value.

Second, we estimated Δt for the same wedge to propagate around the tank by taking the difference in time between every other turbulent patch and calculating $480/\Delta t$. These results are shown in Figure 8. In this figure, we see a much more stable estimate of the actual phase speed than we observed in Figure 7. The reason for the more stable estimate in Figure 8 is that we are following the same turbulent region all the way around the tank rather than simply estimating the phase speed by using the time between successive patches. In Figures 7 and 8, we show two estimates of phase speed for the one-wave case because, in the two-wave case, we can only estimate phase speeds by using the time between successive patches, as in Figure 7. The reason for this is that, in the two-wave case, the turbulent regions may not propagate all the way around the tank since the bottom forcing is not steady in time when viewed from the frame of reference attached to the turbulent region, unlike the forcing in the one-wave case. Thus, in the two-wave

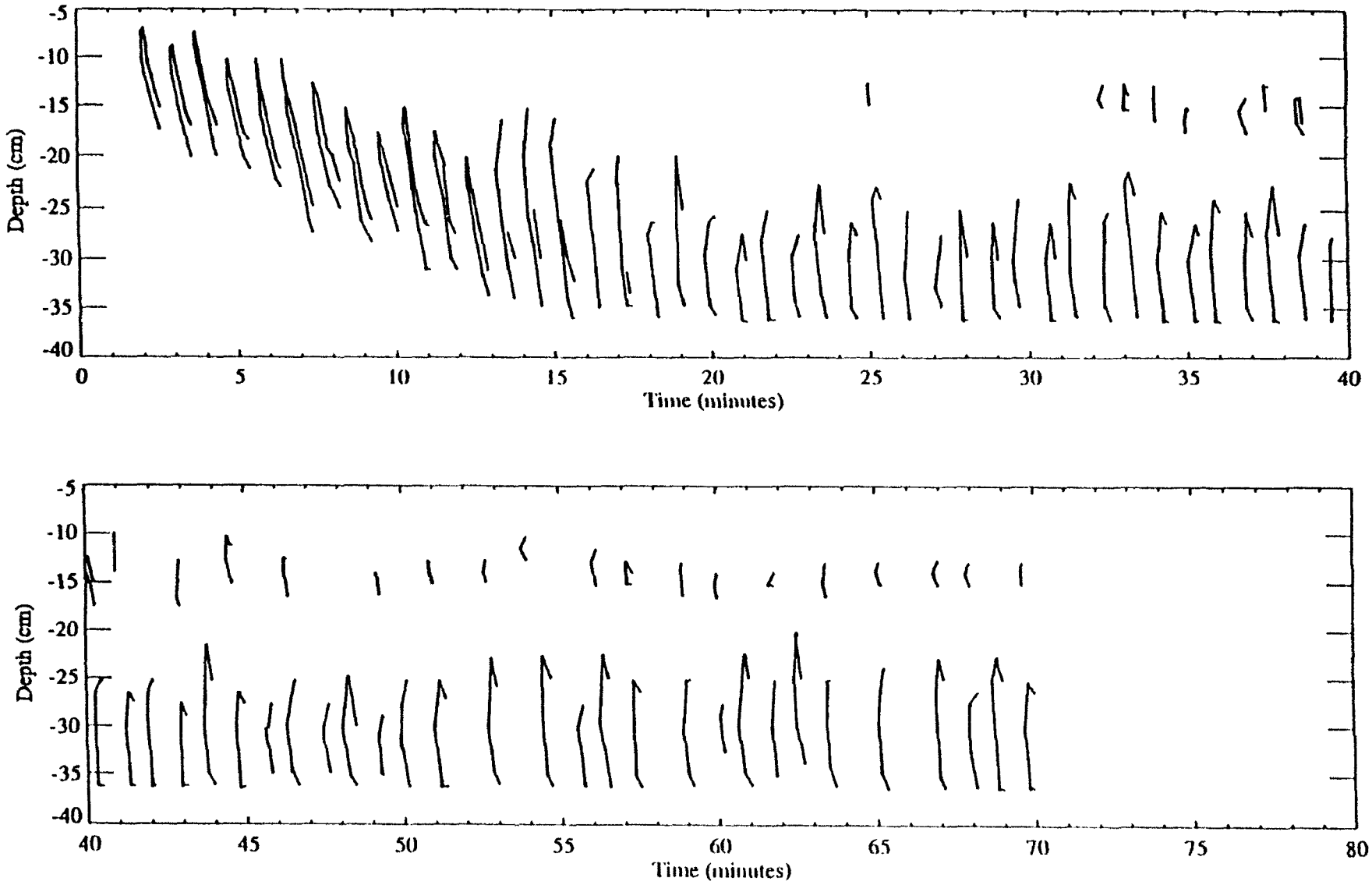

Figure 6. Observed regions of turbulence in the one-wave case (depth vs. time after the start of the experiment).

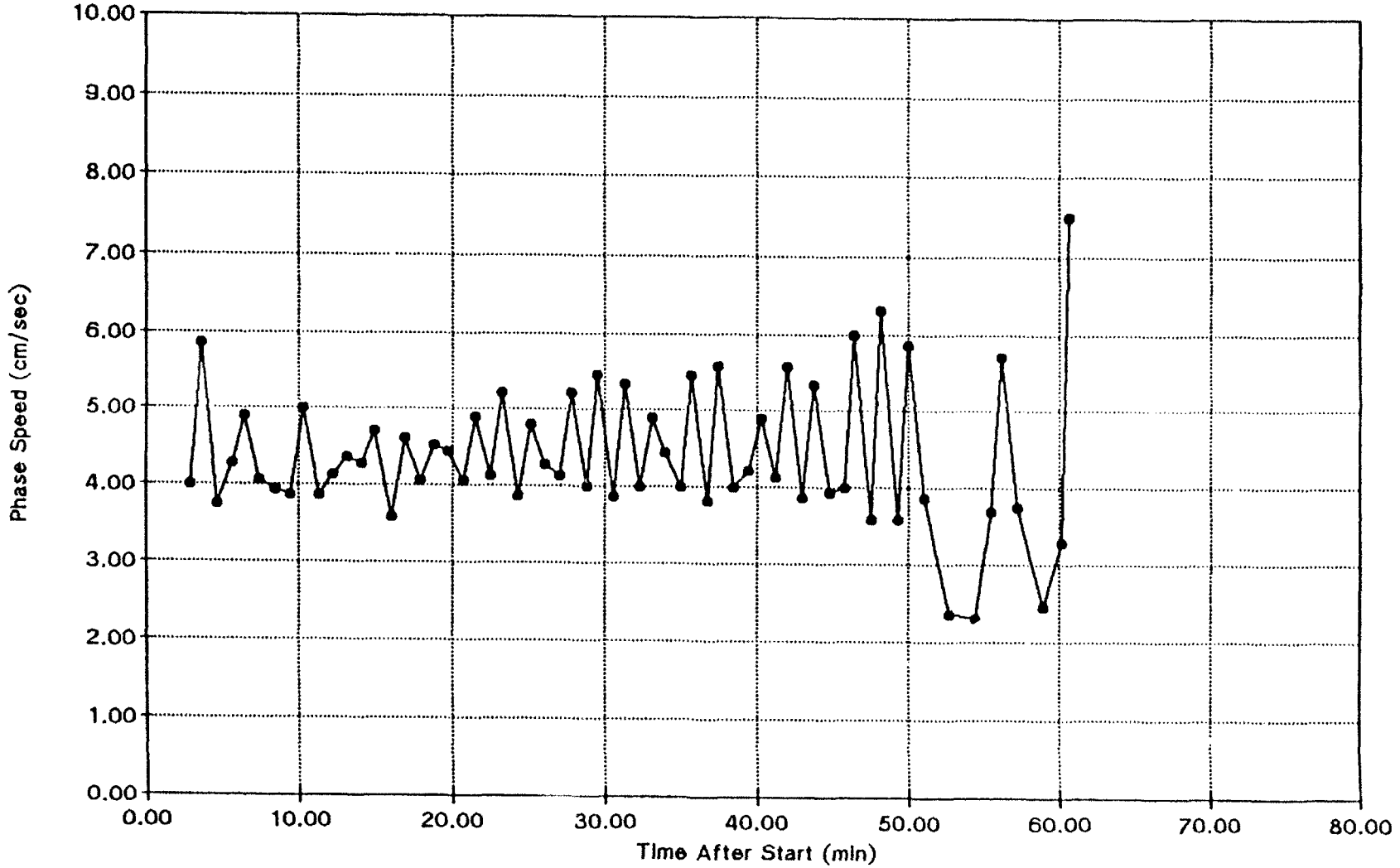

Figure 7. Phase speed for the one-wave case estimated from the observed time of the initial turbulence in each patch. The input phase speed of the bottom floor wave was 4.50 cm/sec; the measured phase speed was 4.48 cm/sec.

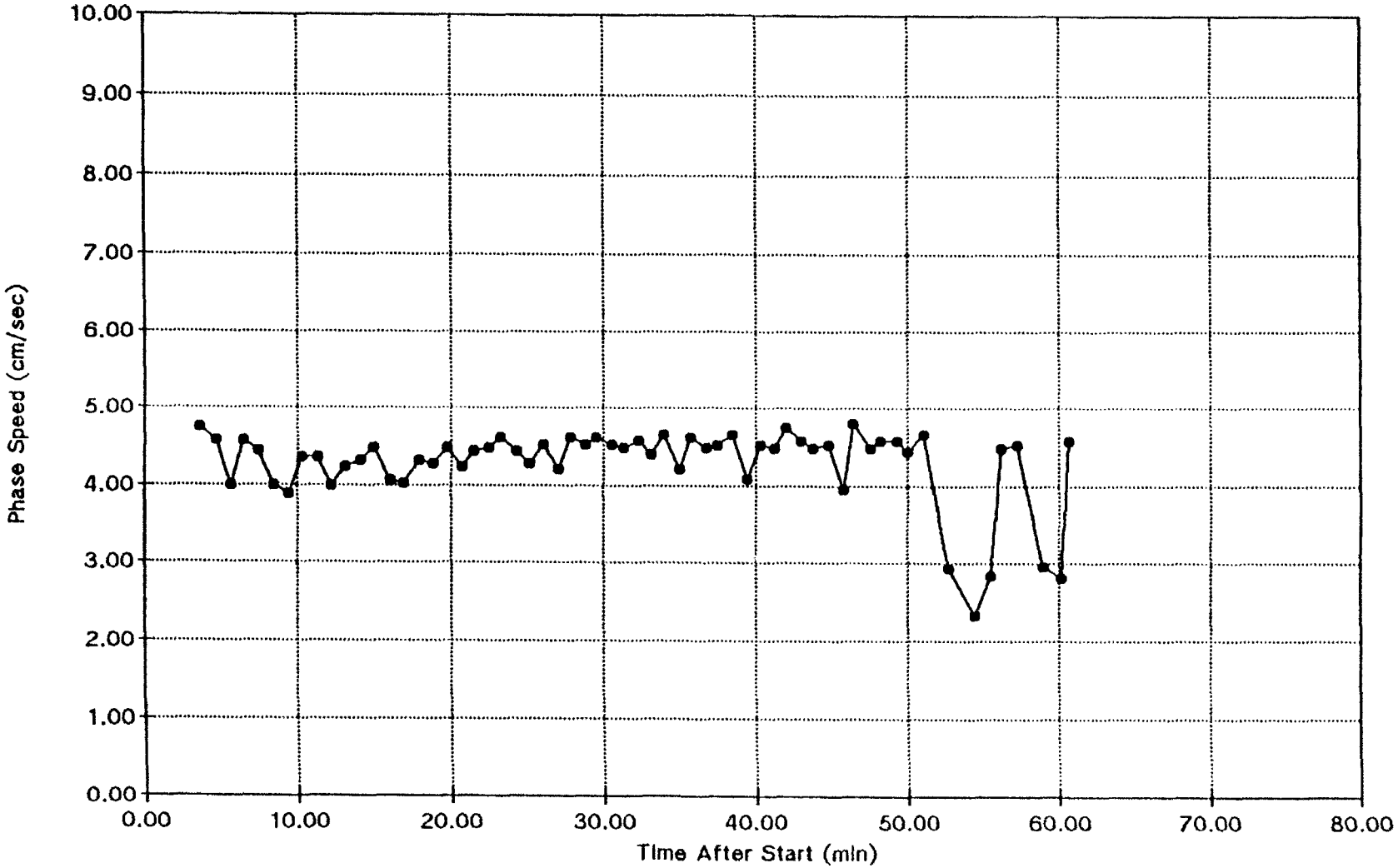

Figure 8. Phase speed for the one-wave case estimated from the observed time of the initial turbulence in every other patch. The input phase speed of the bottom floor wave was 4.50 cm/sec; the measured phase speed was 4.48 cm/sec.

case, the variance in phase speed will be more like that shown in Figure 7, even though the actual phase speed is a constant.

Finally, we note in Figure 8 that in the K-H breaking region ($t \lesssim 13$ min), the estimate of phase speed is not nearly as constant as it is later in the run (e.g., for t between 20 and 50 min). We suspect this is because, as time increases, the K-H breaking region progresses more and more towards the bottom floor of the tank, and does not occur at the same phase of the bottom wave. This has the effect of reducing the calculated phase speed. Only when the turbulent region is nearly steady state in depth does the turbulence appear to have "locked on" to the forcing wave, yielding a nearly constant phase speed.

4.3.2 Two Wave Results

In this section, we discuss our two-wave experimental results. In this case, the two waves had the following parameters:

WAVE	WAVENUMBER	AMPLITUDE (PEAK-TO-PEAK)	SPEED
1	2	3.0 cm	4.5 cm/sec
2	2	3.0 cm	3.5 cm/sec

Figure 9 shows the measured height of the bottom floor at one location for this case. Here, the forcing waves at the floor were initially started at zero amplitude, and the amplitudes were gradually increased to the maximum values after four revolutions around the tank, at a time of about 7 minutes. In this case, the bottom floor repeats itself every 8 minutes, and not every wave cycle, as in the one-wave case (cf., Figure 5).

We show the two-wave case schematically in Figure 10. Here the vertical axis is time in minutes and the horizontal axis is distance in centimeters. Lines of constant phase are shown for both the 4.5 cm/sec wave (Wave 1) and the 3.5 cm/sec wave (Wave 2). If we interpret the phase line of Wave 1 to be a wavecrest and the phase line of Wave 2 to be a trough, then no deflection of the bottom floor should occur when these two phase lines cross, since the crest of Wave 1 would exactly cancel the trough of Wave 2, since the amplitudes are equal. This condition occurs at the time-space position marked a on Figure 10. The next time exact cancellation occurs at the same position in the tank (multiples of 480 cm from position a) is at the time-space position marked b on Figure 10. This cancellation occurs exactly 8 minutes after the first cancellation.

The pattern shown in Figure 10 can be observed in the measurements shown in Figure 9. Note in Figure 9 that the bottom floor has practically no vertical motion at times of 10, 18, 26, 34, 42, 50, 58 and 66 minutes after the start of the experiment, and that these times are 8 minutes apart.

Figure 11 shows the breaking regions as a function of time for the two-wave case. For early time, $t \lesssim 13$ min, the shadowgraph visualizations show that the breaking regions are K-H. Figure

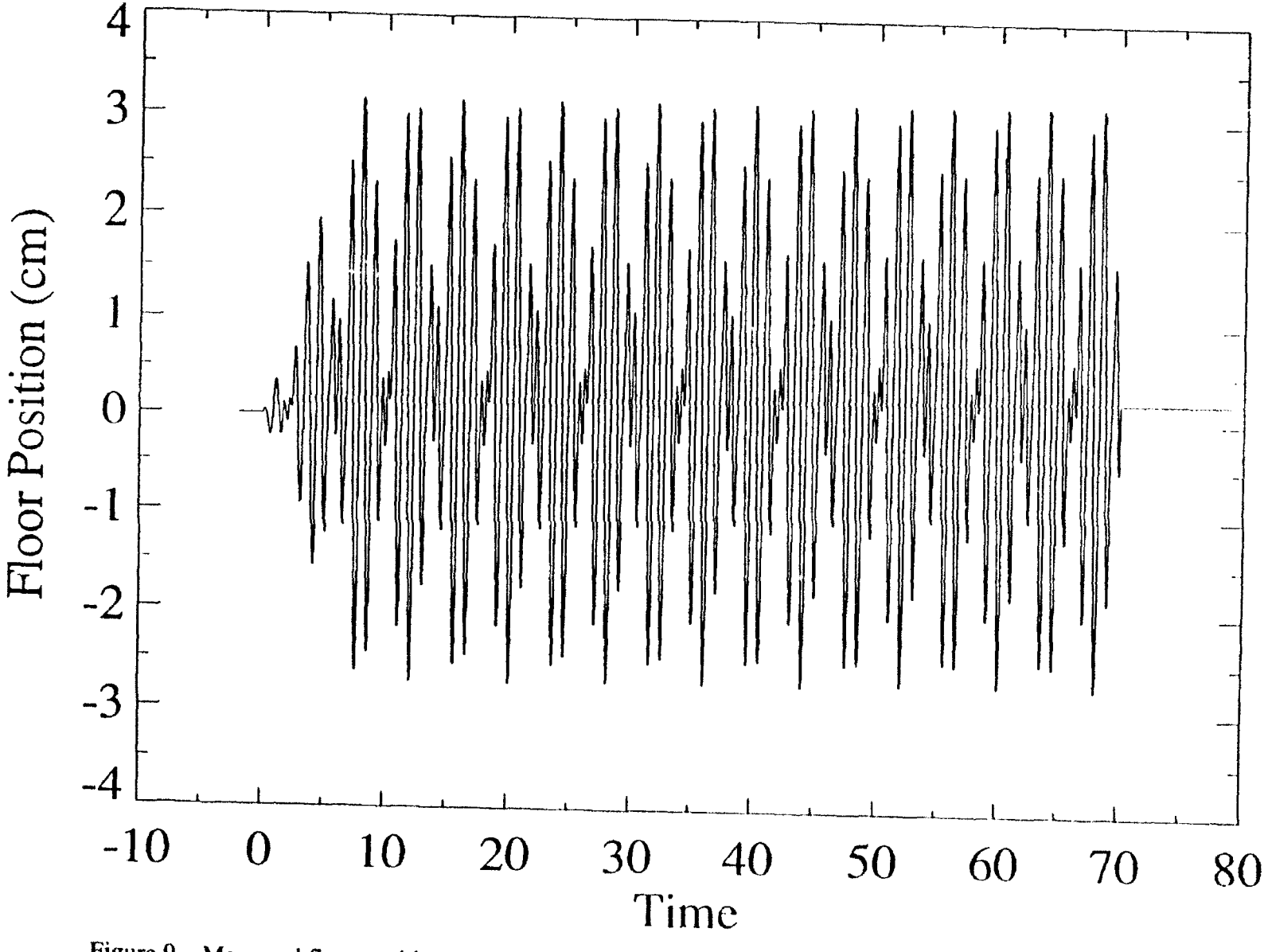

Figure 9. Measured floor position (cm) vs. time (sec) at one location for the two-wave case.

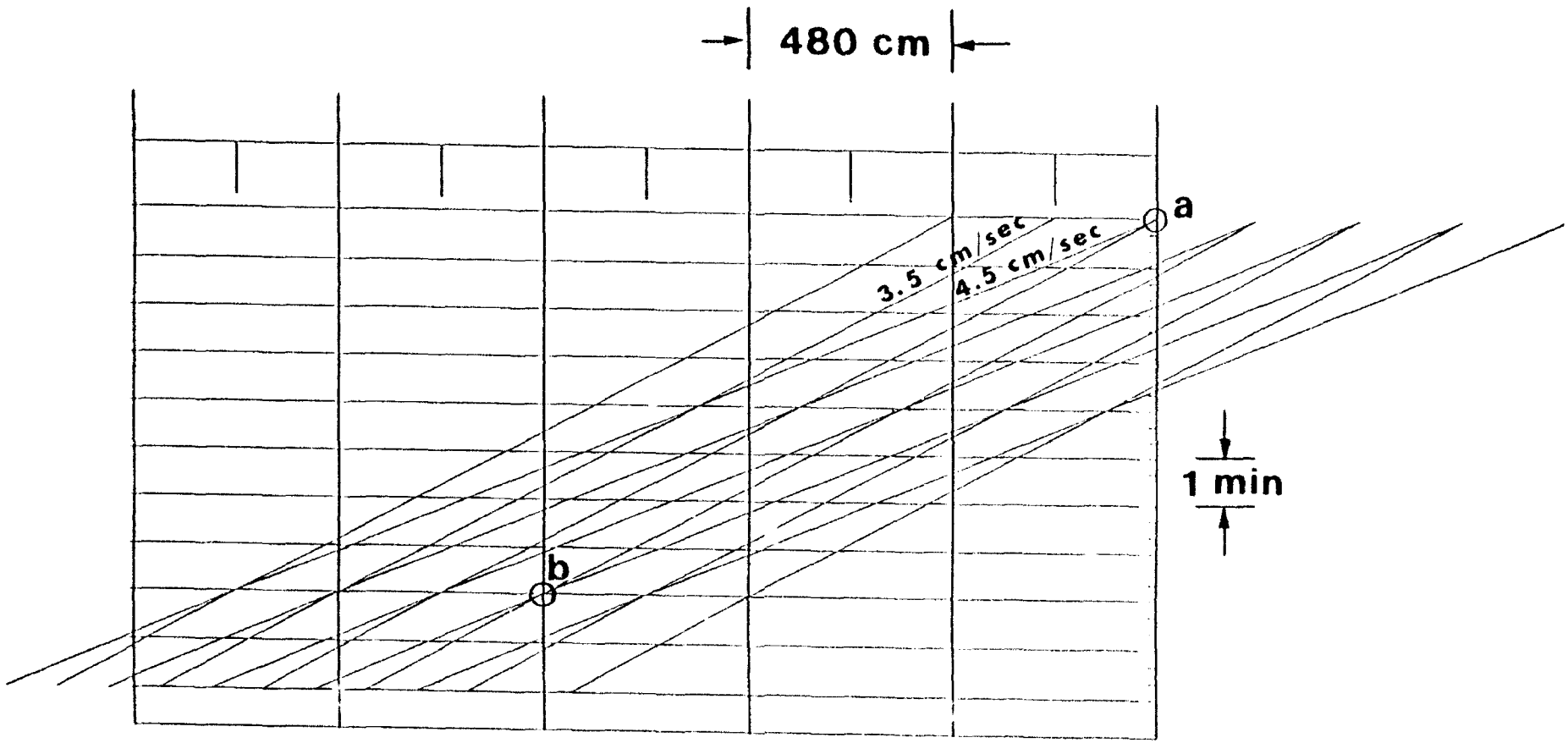

Figure 10. Time-space plot of the two-wave case. At the same position in the tank, cancellation occurs at point a and point b, separated by 8 minutes.

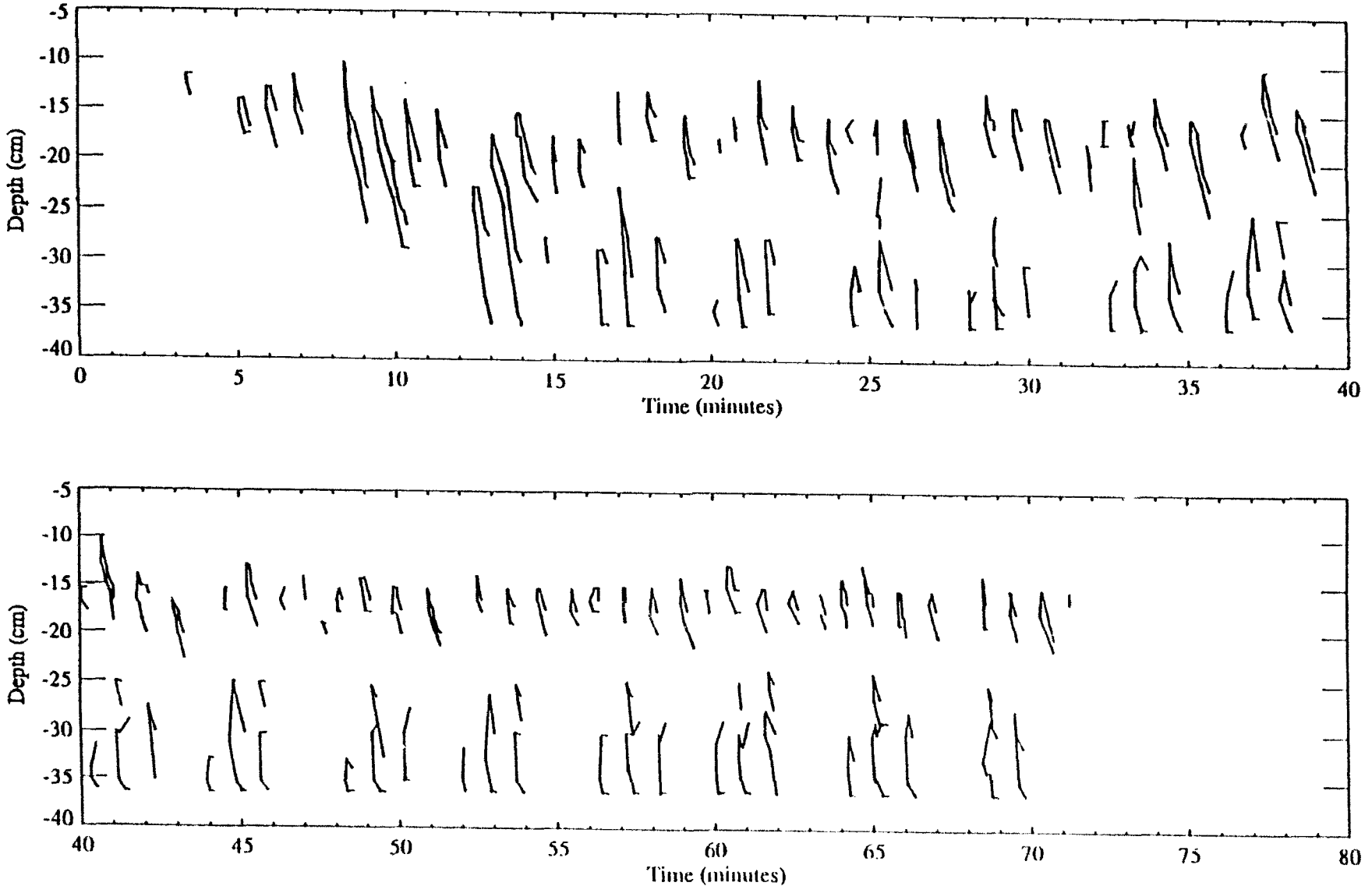

Figure 11. Observed regions of turbulence in the two-wave case (depth vs. time after the start of the experiment). Compare with Figure 6.

11 shows an early pattern of breaking similar to the pattern shown for the one-wave case (Figure 6) in that the breaking regions occur initially high up in the tank and progress towards the floor of the tank with time. (The lack of wave breaking before t ~ 5 min. is probably attributable to the ramping up of wave amplitudes in Figure 11 vs. Figure 6 where the waves started at full amplitude at t = 0.)

At t ~ 13 min, a significant difference occurs between the one-wave and the two-wave cases. In the one-wave case (Figure 6), the "wedge" forms near the bottom of the tank and appears once every wave cycle. Only small, sporadic turbulence is observed above the wedge, at depths around 15 cm. In the two-wave case (Figure 11), around t ~ 13 min, the turbulent regions appear to bifurcate, with K-H breaking appearing at a depth around 17 cm and a wedge appearing in the lower portion of the tank. The K-H regions in the upper part of the tank appear more or less periodically. This is in contrast to the wedges in the bottom of the tank, which appear in packets of three. In Figure 11, there is turbulence at nearly all depths of the wave tank at t = 17, 25, and 33 minutes. These times are eight minutes apart, and correspond to just before the times of no vertical motion of the tank bottom (cf., Figure 9). The packets of three bottom wedges correspond to the two wave packets in between no motion of the bottom floor, as seen in Figure 9.

Estimates of the phase speed of the turbulent regions in the top and bottom of the tank are shown in Figures 12 and 13, respectively. These estimates were obtained using the time between successive turbulent regions, as in Figure 7. In Figure 13, we did not compute a phase speed based on the long time gaps between wave packets. While the scatter is significant in these figures, one's overall impression is that both the top and bottom regions are being influenced by both waves. For example, in both figures, there are many estimated wave speeds at 3.5 and 4.5 cm/sec. Also, note in Figure 11 that the K-H wave breaking in the top of the tank is stronger (longer lasting) and more periodic than the wave breaking in the top of the tank for the one-wave case (Figure 6), even though the amplitude of the faster wave in Figure 11 is smaller than the amplitude of the same wave in Figure 6. Our speculation is that mean flow modifications are not occurring nearly as rapidly in the two-wave case as in the one-wave case. Thus, we believe the wave energy is still able, at long times, to propagate up into the tank and to generate overturning at higher levels than was observed in the one-wave case. It is also possible that this wave energy is being allowed to propagate upwards only during times when the wedges are not occurring in the bottom of the tank. We believe examination of the instantaneous and mean velocity profiles may shed some light on these observations. These velocity profiles are being examined now.

5. Plans for the Next Year

During the next year, we intend to examine the following:

a. We will examine the instantaneous and mean velocity profiles to determine the mean flow accelerations in all two-wave cases,

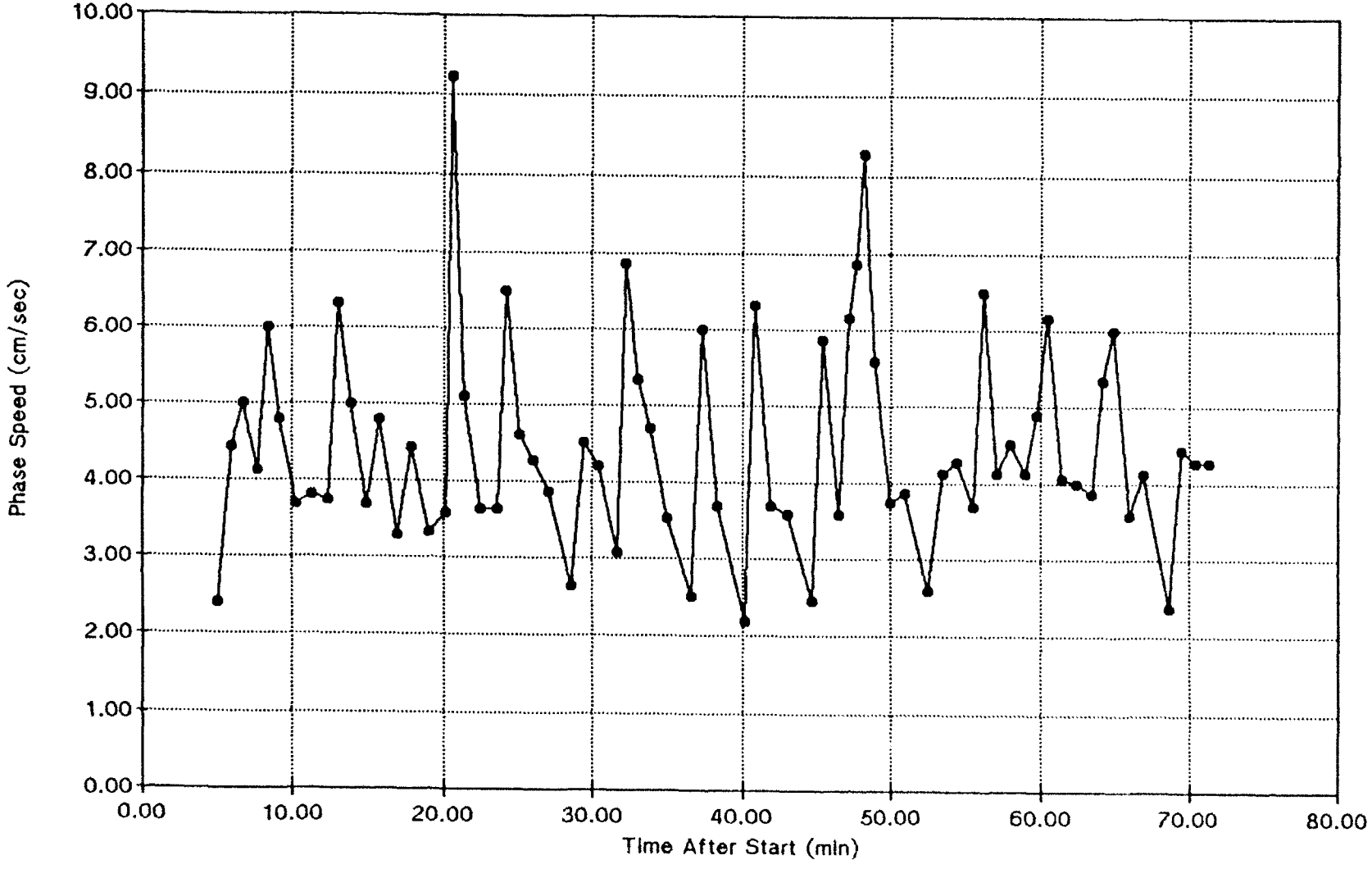

Figure 12. Phase speed in the top of the tank for the two-wave case, estimated from the observed time of the initial turbulence in each patch.

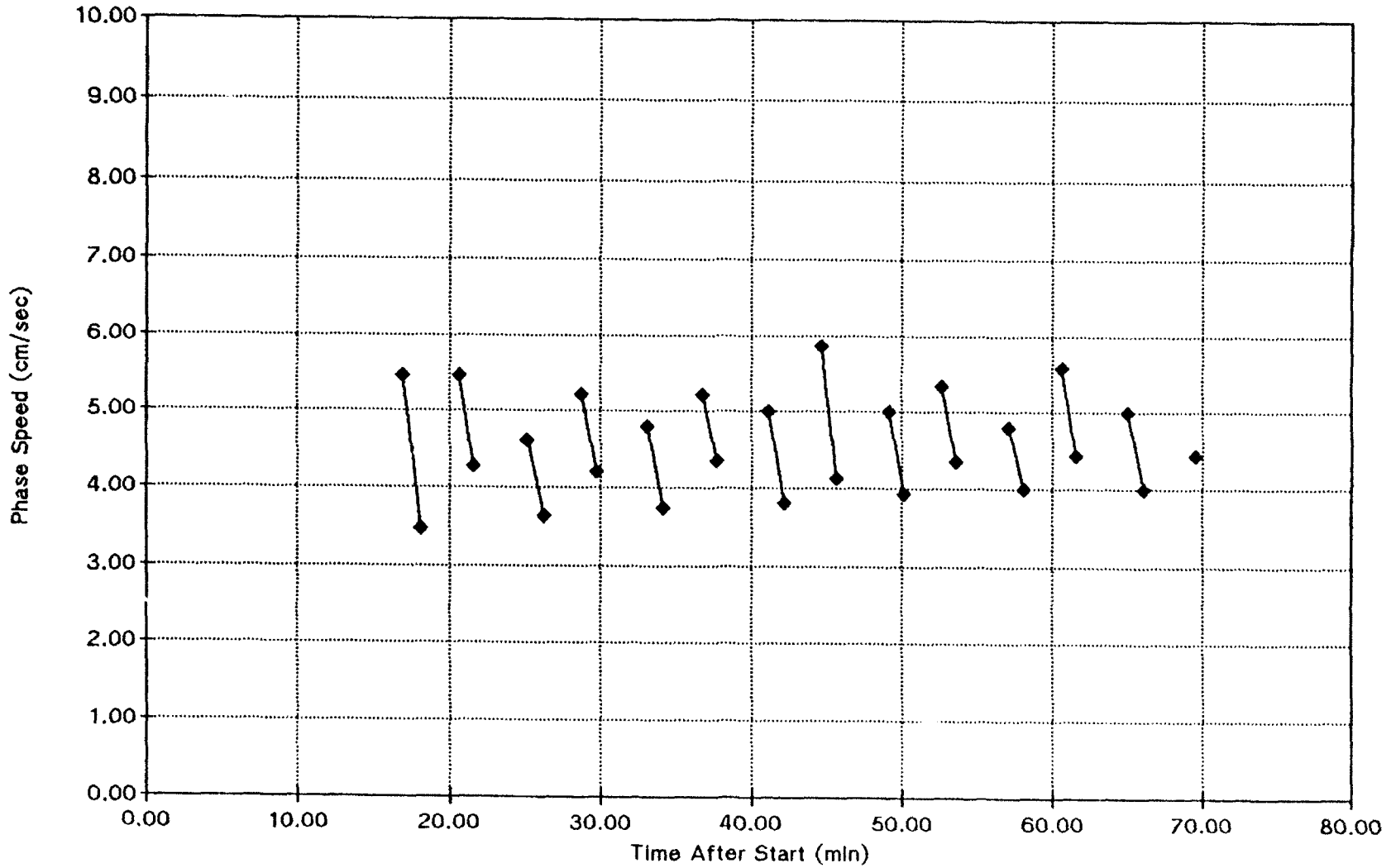

Figure 13. Phase speed in the bottom of the tank for the two-wave case, estimated from the observed time of the initial turbulence in each wedge. Estimates are shown only for wedges within each packet.

b. We will perform more two-wave experiments with smaller and larger amplitudes of Wave 2 to determine the effect of amplitude,

c. We anticipate decreasing the stratification in the bottom layer to determine the effect of increasing the dissipation scale height,

d. We anticipate increasing and decreasing the phase speed of Wave 2 to determine the effect of changing the vertical separation of critical layers, and

e. W expect to begin preparations for examining critical layers due to a compact wave source.

The results of these experiments will be discussed in next year's report.

REFERENCES

Andrews, D.G., J.R. Holton, and C.B. Leovy , 1987: Middle Atmosphere Dynamics. Academic Press, New York.

Benney, D.J. and R.F. Bergeron, 1969: A New Class of Nonlinear Waves in Parallel Flows. Stud. Appl. Math., 48, 181-204.

Booker, J.R. and F.P. Bretherton, 1967: The Critical Layer for Internal Gravity Waves in a Shear Flow. J. Fluid Mech., 27, 513-539.

Bretherton, F.P., 1966: The Propagation of Internal Gravity Waves in a Shear Flow. Quart. J. Roy. Meteor. Soc., 92, 446-880.

Bretherton, F.P., P. Hazel, S.A. Thorpe, and I.R. Wood, 1967: Appendix to the paper by P. Hazel, The Effect of Viscosity and Heat Conduction on Internal Gravity Waves at a Critical Level. J. Fluid Mech., 30, 775-783, (Appendix on pp. 781-783.)

Brown, S.N. and K. Stewartson, 1980: On the Nonlinear Reflextion of a Gravity Wave at a Critical Level. Part 1. J. Fluid Mech., 100, 557-595.

Delisi, D.P., 1988: Studies of Internal Wave/Mean Flow Interactions. Northwest Research Associates Report NWRA-CR-88-R029, Bellevue, WA.

Delisi, D.P. and T.J. Dunkerton, 1989: Laboratory Observations of Gravity Wave Critical-Layer Flows. Pure and Appl. Geophys., 130, 445-661.

Dunkerton, T.J., 1980: A Lagrangian Mean Theory of Wave, Mean-flow Interaction with Applications to Nonacceleration and its Breakdown. Rev. Geophys. Space Phys., 18, 387-400

Dunkerton, T.J. 1981: Wave Transcience in a Compressible Atmosphere, Part I: Transient Internal Wave, Mean-Flow Interaction. J. Atmos. Sci., 38, 281-297.

Dunkerton, T.J., 1982: Wave Transience in a Compressible Atmosphere, Part 3: The Saturation of Internal Gravity Waves in the Mesosphere. J. Atmos. Sci., 39, 1042-1051.

Dunkerton, T. J. and D. C. Fritts, 1984: The Transient Gravity Wave Critical Layer, Part 1: Convective Adjustment and the Mean Zonal Acceleration. J. Atmos. Sci., 41, 992-1007.

Fritts, D.C., 1978: The Nonlinear Gravity Wave-Critical Level Interaction. J. Atmos. Sci., 35 397-413.

Fritts, D.C., 1979: The Excitation of Radiating Waves and Kelvin-Helmholtz Instabilities by the Gravity Wave-Critical Layer Interaction. J. Atmos. Sci., 36, 12-23.

Fritts, D. C., 1982: The Transient Critical-Level Interaction in a Boussinesq Fluid. J. Geophys. Res., 87, 7997-8016.

Fritts, D. C., 1984: Gravity Wave Saturation in the Middle Atmosphere: A Review of Theory and Observations. Rev. Geophys. Space Phys., 22, 275-308.

Grimshaw, R., 1975: Nonlinear Internal Gravity Waves and Their Interaction with the Mean Wind. J. Atmos. Sci., 32, 1779-1793.

Koop, C. G., 1981: A Preliminary Investigation of the Interaction of Internal Gravity Waves With a Steady Shearing Motion. J. Fluid Mech., 113, 347-386.

Koop, C. G. and B. McGee, 1986: Measurements of Internal Gravity Waves in a Continuously Stratified Shear Flow. J. Fluid Mech., 172, 453-480.

Lindzen, R.S., 1981: Turbulence and Stress Owing to Gravity Wave and Tidal Breakdown. J. Geophys. Res., 86, 9707-9714.

Maslowe, S.A., 1973: Finite-Amplitude Kelvin-Helmholtz Billows. Bound-Layer Meteor., 5, 43-52.

Maslowe, S.A., 1977: Weakly Nonlinear Stability Theory of Stratified Shear Flows. Quart. J. Roy. Meteor. Soc., 103, 769-783.

Maslowe, S.A., 1986: Critical Layers in Shear Flows. Ann. Rev. Fluid Mech., 18, 405-432.

Nastrom, G.D., D.C. Fritts, and K. S. Gage, 1987: An Investigation of Terrain Effects on the Mesoscale Spectrum of Atmospheric Motions. J. Atmos. Sci., 44, 3087-3096.

Plumb, R.A. and A.D. McEwan, 1978: The Instability of a Forced Standing Wave in a Viscous Stratified Fluid: A Laboratory Analogue of the Quasi-Biennial Oscillation. J. Atmos. Sci., 35, 1827-1839.

Thorpe, S. A., 1973: Turbulence in Stably Stratified Fluids: A Review of Laboratory Experiments. Boundary-Layer Meteorol., 5, 95-119.

Thorpe, S. A., 1981: An Experimental Study of Critical Layers. J. Fluid Mech., 103, 321-344.